

Diffusion Counterfactuals for Image Regressors

Trung Duc Ha^[0009–0001–2461–6833] and Sidney Bender^[0009–0007–1727–8577]

Technische Universität Berlin, Straße des 17. Juni 135, 10623 Berlin, Germany
{t.ha,s.bender}@tu-berlin.de

Abstract. Counterfactual explanations have been successfully applied to create human interpretable explanations for various black-box models. They are handy for tasks in the image domain, where the quality of the explanations benefits from recent advances in generative models. Although counterfactual explanations have been widely applied to classification models, their application to regression tasks remains underexplored. We present two methods to create counterfactual explanations for image regression tasks using diffusion-based generative models to address challenges in sparsity and quality: 1) one based on a Denoising Diffusion Probabilistic Model that operates directly in pixel-space and 2) another based on a Diffusion Autoencoder operating in latent space. Both produce realistic, semantic, and smooth counterfactuals on CelebA-HQ and a synthetic data set, providing easily interpretable insights into the decision-making process of the regression model and reveal spurious correlations. We find that for regression counterfactuals, changes in features depend on the region of the predicted value. Large semantic changes are needed for significant changes in predicted values, making it harder to find sparse counterfactuals than with classifiers. Moreover, pixel space counterfactuals are more sparse while latent space counterfactuals are of higher quality and allow bigger semantic changes.

Keywords: Counterfactual Explanations · Diffusion Models · Image Regression.

1 Introduction

Interpreting the results of deep learning (DL) models is still challenging due to the black-box nature of the predictions. In particular, the model might be using features that indicate good performance while completely relying on spurious correlations, commonly referred to as the “clever hans effect” [1, 35, 51, 52]. In addition, understanding these results is critical for ethical and safety reasons in fields such as healthcare, credit scoring, and more. DL models must guarantee trustability, transparency, and fairness to be deployed in these areas [12].

This paper will focus on the post hoc explanation method called *counterfactual explanations*. The goal is to provide a “what-if” scenario of an alternate input that changes the prediction of the model while constraining the changes to be minimal and semantically meaningful [16]. This creates counterexamples that are more likely to be intuitive and easily interpretable [59]. Thus, users may

arrive at natural conclusions such as “had I only changed X , the system would have predicted Y' rather than Y .”

Particular interest has been given to image counterfactuals using generative models, guided by gradients toward altering the prediction. These methods can be divided into two categories: Using latent representations [14, 48] or derivatives of diffusion models [2, 24, 25, 26] to create changes along the data manifold. The effectiveness of these methods hinges on image quality, leading to increased adoption of diffusion models.

Most CE methods focus on image classification, as in the previous work mentioned. However, many important image tasks involve regression, especially in pathology [17, 10, 53, 58]. Explainable AI for Regression (XAIR) methods have emerged to form a theoretical foundation [29, 36, 37, 38]. Specifically, selecting an appropriate reference point is essential for producing the right explanations. In the context of XAIR, this is referred to as the *reference value* [38]. It serves as an important parameter for the context of a regression explanation, e.g. “what would this person look like if they were 20 or 80 years old?”. This approach allows for more targeted explanations, distinguishing it from classifier explanations.

Some counterfactual approaches for image regression exist [2, 14]. However, these approaches either use low-resolution generative models or do not use pre-trained regressors. Moreover, they do not consider reference values. This gap forms the foundation of the contributions of this paper. Image regression counterfactuals present unique challenges: How do we achieve minimal, meaningful, and realistic changes while applying them effectively to regression? Moreover, defining minimality through pixel footprint may decrease interpretability [13].

To address these issues, our contributions are twofold: (1) We present two methods to create counterfactual explanations for image regression tasks using diffusion-based generative models. We adapt Adversarial Counterfactual Explanations (ACE) [25] that operate directly in pixel space and the Diffusion Autoencoder (Diff-AE) [45] that operates in latent space. (2) Regression-specific adaptations that allow us to produce counterfactuals with higher granularity, inspecting specific regions of the predicted values.

Our experiments on CelebA-HQ and a synthetic dataset demonstrate that both methods produce realistic, semantic, and smooth counterfactuals. We can reveal spurious correlations and observe that feature changes depend on the prediction region, with larger semantic alterations required for significant value shifts. Furthermore, we find a trade-off between sparsity and quality, with pixel-space changes offering greater sparsity, and latent-space edits providing higher quality and semantic flexibility.

The remainder of this paper is organized as follows. Section 2 reviews the relevant literature on counterfactual explanations and existing regression explanation techniques. Section 3 includes an overview of diffusion models and their derivatives and elaborates on our two novel approaches. Section 4 details our experimental setup with datasets, evaluation methods, and their results. It also includes implementation details, an ablation study, and regression-specific explanation analysis with spurious correlation identification. Finally, Section 5

concludes the paper with a summary of our findings and a discussion of potential future research directions.

2 Related Work

We contextualize our work by reviewing key studies on XAI, counterfactual explanations, and regression explanations relevant to our approach. Furthermore, we highlight the position of our work within the limited research of image regression counterfactuals.

2.1 Counterfactual Explanations for XAI

XAI methods generally align themselves by a mixture of the following properties [12, 16, 44, 51]: The scope of a method describes whether it is applicable to the *global* behavior of the model or to a single *local* data point. Its usage categorizes it as interpretable by design (*intrinsic*) or architecture independent, applying to outputs of pre-trained models (*post-hoc*).

Local post-hoc methods are highly useful in areas such as healthcare and finance [12] as they can be directly applied to deployed blackbox models to explain highly critical decisions. Although common methods belonging to this class [3, 4, 42, 47, 56, 61, 62] visualize the importance of features of a particular prediction, they do not suggest *actionable* insights. Counterfactual explanations (CE) [60] have been developed to solve this gap. CEs create a counterexample of an input that alters the model’s prediction, restricting the changes to be minimal and semantically meaningful. They reveal the most sensitive features in an intuitively interpretable manner. This allows users to understand patterns that influence the model’s decision-making and identify potential vulnerabilities or biases. Moreover, CEs are suitable for finding and removing spurious correlations [5, 25].

In image applications, generated counterfactuals must be realistic and lie on the data manifold. Several approaches exist; DiVE [48] employed a Variational Autoencoders [31] to perform modifications in its latent space, restricting it to the data manifold. Diffeomorphic Counterfactuals [14] also followed this approach, additionally using Generative Adversarial Networks (GAN) to do this task, supplementing it with strong theoretical guarantees. Similarly, STEEX [23] used GANs in conjunction with a semantic map to restrict edits. However, these methods are limited by their generative models, which struggle to create high-resolution images.

Diffusion models [19] addressed this problem, leading to adoption for generating counterfactual images. DiME [24] uses diffusion models to partially noise the image and then guide the denoising process using a classifier. Similarly, ACE [25] starts by only partially noising the image. However, they based their method on adversarial attacks [57] using the diffusion process to filter out non-semantic components. In addition, the authors employ RePaint [41] for further refinement.

Counterfactual generation shares goals with semantic editing: making meaningful changes while maintaining overall structure and coherence. Methods involve GANs [9, 40] and more recently diffusion models [11, 21, 33]. We highlight the Diffusion Autoencoder (Diff-AE) [45], which encodes high-resolution images into an editable semantic latent space while accurately reconstructing them. For interpretability, semantic edits are favored by humans, compared to minimal edits enforced by counterfactual search [13].

2.2 Regression Explanations

Several works apply classification-based attribution methods to regression problems either directly [29, 58] or by first converting the regression task into multi-class classification [6, 34]. Letzgus *et al.* [38] suggest that regression explanation methods need adaptation from classification. Since regression involves real-valued predictions, specifying a *reference value* for the explanation method is crucial to align it with the intention of the user. For example, “why an item is currently valued at 1200 dollars compared to its usual 1000 dollars price” [38]. Therefore, the user can provide context and precisely target the explanation. In addition, the reference value can be integrated into the measurement unit of the regression problem. Applications of this methodology include [37] and [36].

Regression counterfactual explanations have also been employed for regression tasks on structured [55] and multivariate time series [46] data. Applied to images, Dombrowski *et al.* [14] generate counterfactuals on the Mall dataset [8], only minimizing/maximizing the predicted number of pedestrians, and do not cover interpolation between explanations.

Several works cover counterfactuals for ordinal regression on pathological images [10, 32, 53]. We highlight the work of Atad *et al.* [2], who apply this to diffusion models by using the Diff-AE and a regressor predicting in the latent space.

This distinction discerns our contribution: using diffusion models to generate high-quality counterfactual images, and explaining a regressor operating in pixel space while considering reference values.

3 Methodology

In this section, we discuss our methods for the generation of regression counterfactuals. We first briefly summarize and review Denoising Diffusion Probabilistic Models (DDPM) and the relevant derivatives, the Denoising Diffusion Implicit Models (DDIM), and the Diffusion Autoencoder (Diff-AE). Lastly, we suggest two novel approaches to create regression counterfactuals: adaptations for ACE to form Adversarial Counterfactual Regression Explanations (AC-RE) and Diff-AE Regression Explanations (Diff-AE-RE).

3.1 Diffusion Models and their Derivatives

Denosing Diffusion Probabilistic Models (DDPMs) [19] belong to a family of models that learn to model a data distribution through a forward and reverse noising process. The forward process gradually adds Gaussian noise to a data sample \mathbf{x}_0 over timesteps $1 \leq t \leq T$, creating a sequence of increasingly noisy samples. It is possible to directly infer the noised state \mathbf{x}_t from any timestep t as

$$\mathbf{x}_t = \sqrt{\alpha_t} \mathbf{x}_0 + \sqrt{1 - \alpha_t} \epsilon, \quad \epsilon \sim \mathcal{N}(\mathbf{0}, \mathbf{I}). \quad (1)$$

where α_t is the time-dependent noise schedule and ϵ is a noise variable.

A network then learns to reverse this noising process through a Markovian process, starting from $t = T$ and finally reaching \mathbf{x}_0 . This process is computed by

$$\mathbf{x}_{t-1} = \boldsymbol{\mu}_\theta(\mathbf{x}_t, t) + \sigma_t \mathbf{z}, \quad \mathbf{z} \sim \mathcal{N}(\mathbf{0}, \mathbf{I}) \quad (2)$$

where $\boldsymbol{\mu}_\theta(\mathbf{x}_t, t)$ predicts the forward process posterior mean with a network with parameters θ and $\sigma_t \mathbf{z}$ is its deviation at timestep t . We refer the reader to [19] for an in-depth explanation.

Denosing Diffusion Implicit Models (DDIMs) [54] enhance DDPMs by introducing a deterministic approach, while allowing optimization towards the same objective. It modifies the reverse process to only depend on the input and the noise prediction network $\epsilon_\theta(x_t, t)$, directly computing the denoised observation \mathbf{f}_θ :

$$\mathbf{f}_\theta(\mathbf{x}_t, t) = \frac{1}{\sqrt{\alpha_t}} (\mathbf{x}_t - \sqrt{1 - \alpha_t} \epsilon_\theta(\mathbf{x}_t, t)) \quad (3)$$

and resulting in the inference distribution

$$q(\mathbf{x}_{t-1} | \mathbf{x}_t, \mathbf{f}_\theta(\mathbf{x}_t, t)) = \mathcal{N} \left(\sqrt{\alpha_{t-1}} \mathbf{f}_\theta(\mathbf{x}_t, t) + \sqrt{1 - \alpha_{t-1}} \frac{\mathbf{x}_t - \sqrt{\alpha_t} \mathbf{f}_\theta(\mathbf{x}_t, t)}{\sqrt{1 - \alpha_t}}, \mathbf{I} \right) \quad (4)$$

Because it is deterministic, the noise map \mathbf{x}_T can be used to reconstruct images back to their original state, which implies inversion capabilities. This property is suitable for image editing tasks [21] and is advantageous for the generation of accurate counterfactuals.

Diffusion Autoencoders (Diff-AE). A Diffusion Autoencoder (Diff-AE) [45] is an extension of the DDIM and learns a meaningful and decodable representation of an image while leveraging diffusion models for high-quality reconstruction. It encodes an image into a lower-dimensional *semantic subcode* \mathbf{z}_{sem} that captures high-level structured information and a *stochastic subcode* \mathbf{x}_T that encodes fine-grained stochastic details, taking advantage of the deterministic generative process of the DDIM. The DDIM serves as both the encoder for the stochastic code and the decoder for image reconstruction.

The semantic latent code \mathbf{z}_{sem} is computed by the learnable encoder function Enc_ϕ with parameters ϕ

$$\mathbf{z}_{\text{sem}} = \text{Enc}_\phi(\mathbf{x}_0) \quad (5)$$

mapping an input image \mathbf{x}_0 to its high-level semantic representation. The reverse process of the DDIM is then conditioned on this semantic latent code. The authors extend the expression of the denoised observation \mathbf{f}_θ in Equation 3 and the inference distribution in Equation 4 to:

$$\mathbf{f}_\theta(\mathbf{x}_t, t, \mathbf{z}_{\text{sem}}) = \frac{1}{\sqrt{\alpha_t}}(\mathbf{x}_t - \sqrt{1 - \alpha_t}\epsilon_\theta(\mathbf{x}_t, t, \mathbf{z}_{\text{sem}})) \quad (6)$$

To compute the complete denoising process, we use the mean of the inference distribution $q(\mathbf{x}_{t-1}|\mathbf{x}_t, \mathbf{f}_\theta(\mathbf{x}_t, t, \mathbf{z}_{\text{sem}}))$ for $1 \leq t < T$ and refer to the complete reconstruction at $t = 1$ as

$$\hat{\mathbf{x}} = \mathbf{f}_\theta(\mathbf{x}_1, 1, \mathbf{z}_{\text{sem}}) \quad (7)$$

The stochastic code \mathbf{x}_T is obtained by rewriting the generative process such that it predicts the last noise state [45]:

$$\mathbf{x}_T = \sqrt{\alpha_T}\mathbf{f}_\theta(\mathbf{x}_{T-1}, T-1, \mathbf{z}_{\text{sem}}) + \sqrt{1 - \alpha_T}\epsilon_\theta(\mathbf{x}_{T-1}, T-1, \mathbf{z}_{\text{sem}}) \quad (8)$$

As \mathbf{z}_{sem} is a lower-dimensional vector, it possesses a limited capacity to encode stochastic details. Therefore, \mathbf{x}_T is inclined to represent information that was not covered by \mathbf{z}_{sem} , focusing on encoding local variations to optimize the training objective.

Preechakul *et al.* [45] use the semantic latent code \mathbf{z}_{sem} to allow for semantic editing of images. Even when facial features are fit using only linear models, alterations in \mathbf{z}_{sem} produce meaningful transitions. This property forms the basis for generating counterfactuals on this latent code.

3.2 Adversarial Counterfactual Explanations (ACE)

Jeanneret *et al.* [25] utilize the DDPM as a regularizer to transform adversarial attacks into semantically meaningful counterfactual explanations. Adversarial Counterfactual Explanations (ACE) generate counterfactual images by optimizing adversarial perturbations in the image space while filtering high-frequency and out-of-distribution artifacts using a diffusion model.

More specifically, consider $L_{\text{class}}(\mathbf{x}, y)$ as a function that quantifies the match between a sample \mathbf{x} and a class y , typically the cross-entropy loss, which we aim to minimize. Consider a *filtering function* F that constrains a counterfactual \mathbf{x}' to the data manifold of the training images. ACE implements this filtering function using the DDPM. It forward and reverse processes the counterfactual (Eq. 1 and 2) only to a certain depth $t = \tau$ with $1 < \tau < T$. This function is then referred to as F_τ . Applied to the optimization problem, we arrive at $L_{\text{class}}(F_\tau(\mathbf{x}'), y)$. The adversarial attack is applied through F_τ , filtering unwanted artifacts, and

keeping the structure of the image in tact. The result of the optimization is called the *pre-explanation*.

To further refine the pre-explanation, the authors use the RePaint in-painting strategy [41]. Pixel changes are first thresholded with a binary mask to only include the areas highest in magnitude. Then the transitions between the original image and the counterfactual are smoothed out using the DDPM.

ACE provides coherent explanations without requiring modifications to the examined classifier. It surpasses state-of-the-art counterfactual generation techniques across multiple datasets in terms of validity, sparsity, and realism.

3.3 Diffusion Counterfactuals for Image Regressors

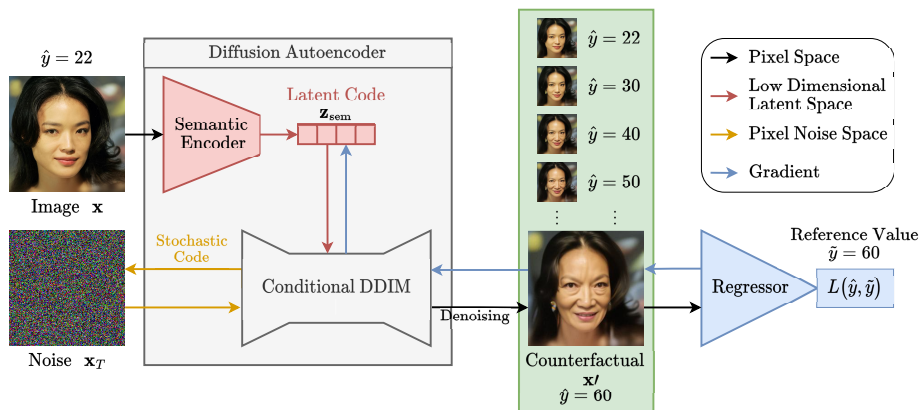


Fig. 1. Diff-AE Regression Explanations (Diff-AE-RE). The Diff-AE encodes an image into two distinct vectors: high-level semantics in the latent code \mathbf{z}_{sem} and low-level features in the stochastic code \mathbf{x}_T . The adversarial attack creates the gradients that only flow towards the latent code. Diff-AE-RE allows for a smooth transition between the counterfactuals across regression values offering fine-grained inspection of changed features

We present the key contribution of this paper: The generation of counterfactual images tied to a regression problem using diffusion models. In Section 2 we discuss two CE generation methods using diffusion-based models: pixel-based and latent space-based. For the pixel space problem we adapt ACE [25], and for the semantic space we use the Diff-AE [45]. Figure 1 presents an overview of the Diff-AE-based method. We refer the reader to [25] for an overview of ACE.

Both methods introduce a loss function targeting the reference value \tilde{y} as described in Section 2, along with a measure of difference from the reference value. We use the Mean Square Error (MSE) for its commonality in regression tasks and the Mean Absolute Error (MAE) for its clarity in interpretation.

Let \mathbf{r}_ψ be a regression model with parameters ψ , \mathbf{x} be a data point, \mathbf{x}' its current counterfactual, initialized to be a copy of \mathbf{x} . The initial prediction of the regressor is given by $\hat{y} = \mathbf{r}_\psi(\mathbf{x}')$ and we assign a designated reference value \tilde{y} . The regression loss function $L_{\text{reg}}(\hat{y}, \tilde{y}) = \text{MSE}(\hat{y}, \tilde{y})$ is the objective of adversarial attacks and $c(\hat{y}, \tilde{y}) = \text{MAE}(\hat{y}, \tilde{y})$ is the difference to the reference value. We empirically choose an early stopping criterion $c \leq 0.05$, similar to the validation error of CelebA-HQ dataset regressors. It balances explanation proximity to \tilde{y} , while limiting optimization steps.

Hence, to produce the counterfactuals \mathbf{x}' we perform the adversarial attack and optimize

$$\arg \min_{\mathbf{x}'} L_{\text{reg}}(\hat{y}, \tilde{y}) \quad \text{s.t.} \quad c(\hat{y}, \tilde{y}) \leq 0.05 \quad (9)$$

To assess the performance of our methods, we use a novel, regression specific metric and established metrics used in ACE [25] and STEEX [23]. We elaborate on the specific details of these metrics in Section 4.

Adversarial Counterfactual Regression Explanations. We adapt ACE using the regression loss described previously L_{reg} . This algorithm performs the prediction on the pre-explanation, $\hat{y} = \mathbf{r}_\psi(F_\tau(\mathbf{x}'))$. The optimized loss function becomes $L_{\text{reg}}(\hat{y}, \tilde{y})$, using the mentioned early stopping criterion. The final refinement stage is performed after a successful adversarial attack. We refer to this regression-specific adaption as *AC-RE*. We expect the same properties of ACE to apply to AC-RE as well, namely semantic changes in the images on the data manifold with filtered out-of-distribution noise. In contrast to ACE, we cannot use a distance function for enhanced sparsity. During empirical testing, we found that the distance function is too limiting to produce counterfactuals that change the predicted value.

Diff-AE Regression Explanations. To adapt Diff-AE we use only the semantic code \mathbf{z}_{sem} to optimize toward the reference value. For the counterfactual \mathbf{x}' we produce its reconstruction $\hat{\mathbf{x}}'$ using the denoising process explained in Section 3.1. With this, the predicted regression value becomes $\hat{y} = \mathbf{r}_\psi(\hat{\mathbf{x}}')$. We then perform an adversarial attack w.r.t. \mathbf{z}_{sem} using the regression loss $L_{\text{reg}}(\hat{y}, \tilde{y})$ until we reach the early stopping criterion. We call this method *Diff-AE-RE*. As we are only attacking the latent space of \mathbf{z}_{sem} , we aim to change only the high-level features of the images.

To enforce semantic sparsity, we add a distance function d between the latent code of the input image and the counterfactual to the objective of the adversarial attack. Through empirical tests elaborated in Section 4.7, we choose the distance function to be the ℓ_1 -distance with its regularization constant $\lambda_d = 10^{-5}$. Let \mathbf{z}_{sem} be the latent code of the input image \mathbf{x} and \mathbf{z}'_{sem} the latent code of the counterfactual \mathbf{x}' . We arrive at the following extended objective:

$$\arg \min_{\mathbf{z}'_{\text{sem}}} L_{\text{reg}}(\hat{y}, \tilde{y}) + \lambda_d d(\mathbf{z}_{\text{sem}}, \mathbf{z}'_{\text{sem}}) \quad \text{s.t.} \quad c(\hat{y}, \tilde{y}) \leq 0.05 \quad (10)$$

This approach is similar to and heavily inspired by approximate diffeomorphic counterfactuals [14], which demonstrate strong theoretical properties for autoencoders. We suggest an analysis of the implications for Diff-AE as future work.

4 Experiments

We experimentally evaluate the effectiveness of our methods in both synthetic and real-world scenarios. We compare their performance against classifier-based approaches and analyze their ability to provide meaningful regression-specific explanations.

First, we describe the datasets used in our experiments, which include a synthetic dataset and CelebA-HQ. We elaborate on the metrics evaluated on these datasets, covering validity, realism, and sparsity. We then outline the implementation details of our methods, specifying how we use the diffusion and regression models. Next, we present quantitative results, comparing our algorithms with classifier-based counterfactual generation approaches. We complement this with qualitative results, providing visual examples of our generated counterfactuals. Additional examples illustrate our models’ ability to reveal spurious correlations and produce fine-grained regression-specific explanations. Finally, we conduct an ablation study that examines the contributions of key components to our methods.

4.1 Datasets

We first test the algorithms on a synthetic dataset called the square dataset. It consists of 64×64 images that have a uniform background from black to white and contains a square of size 8×8 in varying shades of red, enclosed by a gray border. The regression task is to predict the red intensity of the square. This results in a latent space with two dimensions that we can directly control. A minor amount of random Gaussian noise is added to the images to serve as regularization. The objective is to achieve a gradual transition in the color of the square, either from dark to bright red or the reverse. We choose the reference value inversely to the square’s red intensity: darker red squares have bright red reference values, and vice versa. This ensures a balanced contrast for evaluating transitions. By construction, this dataset allows for precise control of particular evaluation aspects, as detailed in Section 4.2.

Following recent literature on generative CE [23, 24, 25], we evaluate our algorithms using the CelebA-HQ dataset [27]. It contains images of size 256×256 of cropped human faces. We choose the attribute “age” to generate the counterfactuals. If a face is marked as “young” we choose the reference value $\tilde{y} = 80$, while we assign “old” $\tilde{y} = 10$ to create CEs that are sufficiently distinct. We normalize ages to a 0-1 range for model training and evaluation.

To train a regression model for age prediction, we use the imdb-wiki-clean dataset [39], a cleaned version of the imdb-wiki dataset [50]. It consists of more

than 500,000 face images with gender and age labels, with the latter being the target of the regressor. The images were cropped to match the CelebA-HQ format.

4.2 Evaluation Methods

We follow Jeanneret *et al.* [25] and assess CEs validity, sparsity, and realism.

The *validity of the explanations* for classification tasks is commonly measured by the flip rate of the CE produced. As there are no fixed thresholds for regression tasks, we choose the oracle score [22] and adapt it to the regression case. We introduce a secondary regressor with the same architecture as an oracle and compute the MAE between the predictions of the original regressor and the oracle. We refer to this as the *Oracle MAE*, suggesting the adversarial potency between the chosen models. A low score indicates the semantic and model-independent nature of the generated counterfactuals.

We determine *sparsity or proximity* by measuring changes in the 40 binary attributes of the CelebA-HQ dataset between the input image and the CE. The VGGFace2 model [7] predicts all attributes of the image pair and computes the mean number of attributes changed (MNAC). Like Jeanneret *et al.* [25], we use face verification accuracy (FVA) [7] and Face Similarity (FS) [25] to assess facial similarity through the deep features of the VGGFace2 model [7]. FS is defined as the cosine distance between the deep features of a pair of images, while FVA thresholds FS to create a binary output.

We evaluate the *realism* of the counterfactual images employing the commonly used FID [18] between the set of input images and the respective CEs.

For the square dataset, we evaluate CE with the same categories of metrics. However, since we can directly control the underlying parameters of the dataset, we can directly extract the MAE of the color values of the square and the background. The first evaluates validity, while the second evaluates sparsity. To assess realism, we also use the FID.

4.3 Implementation Details

This subsection covers technical details of our two approaches and the utilized regression models. We make our code and models available on GitHub.

Algorithms. To reduce the computational requirements for propagating gradients through the iterative process of the DDPM, ACE employs a "time-step re-spacing mechanism" [25]. This approach reduces the number of steps needed at the cost of decreased quality. Hence, AC-RE uses the same hyperparameters as ACE, using 25 steps to noise and 5 steps to de-noise the image, i.e. $\tau = 5$. We reuse the CelebA-HQ DDPM by ACE for AC-RE. To optimize the counterfactual objective, we follow ACE and use projected gradient descent [43] with a learning rate of $\frac{1}{255}$.

Similarly, we balance this tradeoff with Diff-AE-RE. By default, the underlying DDIM uses 250 implicit forward steps and 20 backward steps. Through empirical observations, we choose $T = 10$ for the reverse process to maintain high quality while allowing larger batch sizes. We use the pre-trained Diff-AE by Preechakul *et al.* [45], which was trained on FFHQ [28]. The cropping methods of FFHQ and CelebA-HQ overlap, allowing us to use the model without further modifications. We optimize the counterfactual objective using Adam [30] with a learning rate of 0.002, further elaborated in Section 4.7.

Regression Models. To train the regression models, we fine-tune the pre-trained classification model used by ACE [25], which is based on DenseNet [20]. To adapt this model to a regression task, we replace the final classification layer of the network with a fully connected layer with a single continuous output while freezing all other model weights during training. Hence, the model reuses its feature extraction capabilities, creating explanations comparable to those of the related works.

We also base the oracle model for the Oracle MAE on the DenseNet architecture. Hvilshoj *et al.* [22] argue that the choice of oracle has a major influence on the final score. We aim to ensure comparability with related works by selecting the same architecture for the oracle. However, adversarial vulnerabilities may transfer between the models if we choose to freeze layers. Hence, we decide to fine-tune the entire model, minimizing this risk.

4.4 Quantitative Comparisons

We analyze our methods with the metrics described in Section 4.2. First, we examine the results of the synthetic square data. Afterward, we assess how the methods compare to the classifier-based methods on CelebA-HQ.

Table 1 shows the results for the square dataset. We observe that AC-RE generally performs better in this task. It produces much sparser CE due to the limitations that ACE imposes on the changes: The structure of the image is mostly intact because of the lower amount of noising, and the final refinement stage further limits the areas that are changed.

In contrast, Diff-AE-RE reconstructs the image only from the semantic and stochastic code from a completely noised image. Because of this, the CEs lose their noise pattern, resulting in a higher FID. Figure 2 shows such an example. Moreover, as the structure of the image is expressed with the semantic code, alterations to it naturally lead to broader changes than AC-RE’s pixel-based approach.

Table 2 shows the CelebA-HQ results for the attribute “age” with the evaluation metrics discussed in Section 4.2 and compares them to related classification methods. Compared to the classification-based methods, the FID of our methods is much higher. This is expected; since the CE for classification only need to cross the decision boundary to be considered successful, regression CE need

Table 1. Quantitative Results for the Square dataset. We show the best performance in bold. AC-RE performs much better in sparsity than Diff-AE-RE

Method	Square MAE	FID	Background MAE
AC-RE	0.13	38.1	0.012
Diff-AE-RE	0.167	121.9	0.032

to traverse a significant distance on the loss surface to approach the chosen reference values. Despite this, AC-RE still produces sparse CEs, indicated by the low MNAC score and the high facial similarity indicated by FVA and FS.

In contrast, Diff-AE-RE seems to produce CEs that are more semantically meaningful and realistic, indicated by the lower Oracle MAE and FID scores. Diff-AE-RE is limited to modifications in the latent space, restricting non-semantic adversarial components in the explanations and enabling wider changes in facial structure and properties.

This factor significantly decreases the performance of FVA and FS in the specific task of age regression. In Figure 2, we present CEs from Diff-AE-RE that provide more convincing explanations than AC-RE when creating a CE for an old person turning young. Aging significantly alters facial structure and skin color due to numerous biological processes. Representing these age-related changes in the counterfactual results in larger pixel changes. This affects the extracted deep facial features of the VGGFace2 model, thus lowering the scores.

Table 2. Quantitative Results for CelebA-HQ. We show the best-performing regression-based method in bold. For reference, we compare the quantitative results of ACE [25] on the ‘‘age’’ attribute and show them in italics. Our methods perform similarly to classifier-based methods. AC-RE again produces much sparser CEs, keeping facial features intact, while Diff-AE-RE produces CEs that are more semantically sound and realistic

Method	Oracle MAE	FID	FVA	FS	MNAC
DiVE [48]	-	<i>33.8</i>	<i>98.2</i>	-	<i>4.58</i>
DiVE ¹⁰⁰ [48]	-	<i>39.9</i>	<i>52.2</i>	-	<i>4.27</i>
STEEX [23]	-	<i>11.8</i>	<i>97.5</i>	-	<i>3.44</i>
DiME [24]	-	<i>4.15</i>	<i>95.3</i>	<i>0.6714</i>	<i>3.13</i>
ACE ℓ_1 [25]	-	<i>1.45</i>	<i>99.6</i>	<i>0.7817</i>	3.20
ACE ℓ_2 [25]	-	<i>2.08</i>	<i>99.6</i>	<i>0.7971</i>	2.94
AC-RE	0.260	30.9	93.1	0.666	2.68
Diff-AE-RE	0.184	26.7	80.1	0.599	3.61

4.5 Qualitative Results

We show a selection of qualitative results in Figure 2 for the squares and CelebA-HQ datasets, with their respective reference values. Similarly to the observations

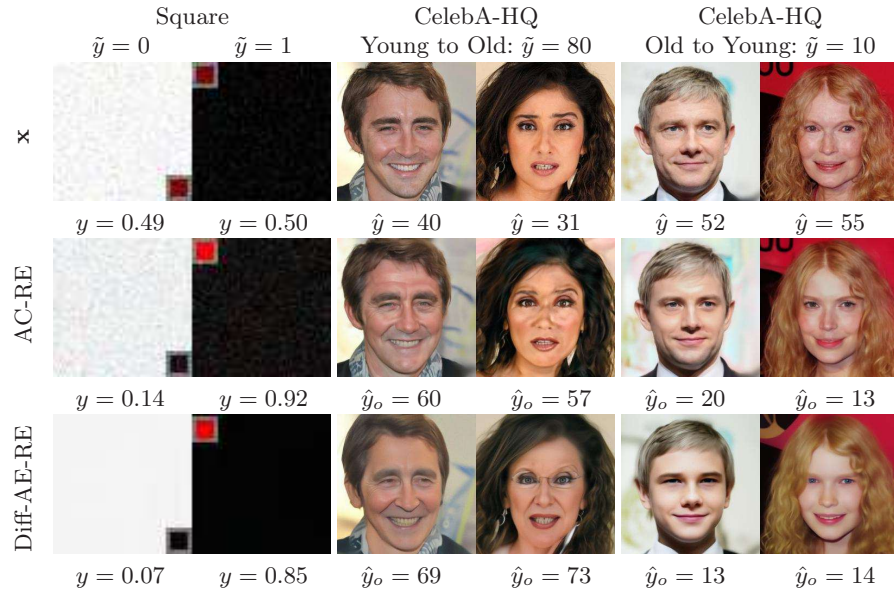


Fig. 2. Qualitative Results. The first row shows the input images \mathbf{x} and their reference values \tilde{y} , while the following rows show the CEs of AC-RE and Diff-AE-RE. The captions indicate the extracted color of the square y , the regressor prediction \hat{y} , or the oracle prediction \hat{y}_o . AC-RE creates sparse explanations, while Diff-AE-RE creates broader and more realistic modifications. For the synthetic dataset, AC-RE creates more accurate counterfactuals. For CelebA-HQ, AC-RE primarily changes the textures in the face. In contrast, Diff-AE-RE alters facial shape, skin and teeth color, and accessories. Its oracle score indicates more realistic changes, aligning closely with the reference values

of the quantitative results in Section 4.4, we see that AC-RE produces sparser CEs, while Diff-AE-RE produces broader changes.

For the square dataset, AC-RE creates a uniform color for the square and even reconstructs the noise patterns. Diff-AE-RE cannot reproduce these patterns, as previously described in Section 4.4. Moreover, the algorithm slightly shifted the location of the square of the image with the darker background (the border is no longer aligned with the edge of the image). Both algorithms perform similarly well regarding altering the actual color of the square.

For CelebA-HQ, AC-RE focuses on texture alterations, such as adding wrinkles and smoothing the skin, staying sparse in the pixel space. Diff-AE-RE introduces more distinct and realistic changes. This is reflected in the predictions of the Oracle model. They align more closely with the reference values, indicating fewer adversarial components. Although these changes are less minimal concerning the changed pixels, we see them as an advantage in creating additional features for interpretability. Specifically, we observe changes in facial shape, skin, and teeth color, and the presence of accessories.

The final point stands out significantly in our observations. For many CEs, we observe that Diff-AE-RE adds glasses or earrings. We investigate these phenomena in more detail to uncover spurious correlations in Section 4.5 and age-range-specific explanations in Section 4.6.

Spurious Correlations of the Regressor. Counterfactual explanations are the most effective when the changes are minimal and actionable. However, the definition of minimality changes depending on the context [16]. While ACE favors minimal pixel changes [25], enforcing it may not faithfully represent the behavior of the model and limit intuitive counterfactuals [13].

Although adding an accessory such as glasses introduces a significant pixel footprint in the image, it is a simple feature to understand for humans. As we observed in Section 4.5, Diff-AE-RE frequently adds glasses to the faces of CelebA-HQ to create a counterfactual of a young person to appear old.

Using this information, we conduct an experiment on a subset of the CelebA-HQ validation set: We use the getimg.ai Image Editor [15] to mask the area around the eyes and inpaint the image with the prompt “a person wearing glasses”. This way, we precisely control the modifications to the image while creating realistic-looking images. Afterward, we compute the difference between the predictions of the regressor for the original and the edited image. We show the results in Figure 3.

We observe that the modifications increase the predicted age by at least about five years, on average seven years. Notably, the edit of the first example has a particularly strong response, increasing the prediction by eleven years. However, the effect seems to be more pronounced for male faces, indicating a potential bias in the training dataset. Using our counterfactuals, we show that suggested feature changes can be directly applied in a very intuitive way (“putting on glasses”) to alter the result of the regression model.

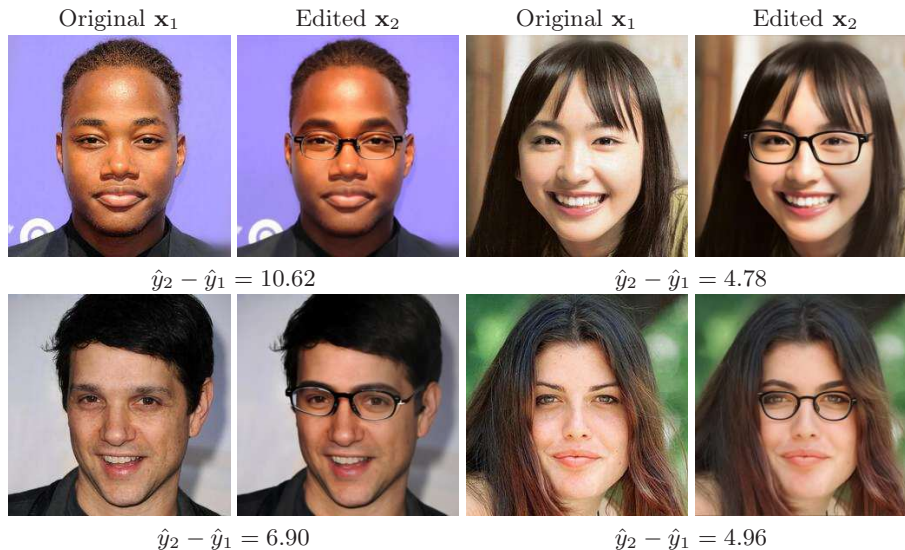


Fig. 3. Spurious Correlation. We reveal a spurious correlation in the regressor for sample images from the CelebA-HQ validation set. We use the getimg.ai Image Editor [15] to add glasses to each person via inpainting. On average, the person appears to be 7 years older than the model, with the first example showing an especially strong change. The effect seems to be more pronounced for male faces

4.6 Regression Specific Explanations

To illustrate the differences between classification- and regression-based CEs, we explain a single image for various reference values, showing granular explanations between age regions. We choose five representative reference values \tilde{y} in the target domain, specifically 10, 20, 40, 60, and 80, and analyze the main feature changes between each.

Figure 4 presents the results of AC-RE and Diff-AE-RE for this experiment, including the reconstructed images and the counterfactuals for each reference value for the two algorithms. Underneath the explanations, we visualize the difference between the reconstruction and its counterfactuals by plotting a heatmap showing the mean pixel value differences across color channels. Red indicates an increase in brightness, while blue indicates a decrease in brightness. For this particular example, the initial prediction of the person is 20 years. This does not result in changes in the counterfactual for Diff-AE-RE for $\tilde{y} = 20$. However, AC-RE performs the refinement step regardless of the predicted value, always producing minor changes in the image.

We first analyze the explanations for AC-RE. As this algorithm produces sparse and subtle changes, the colors of the heatmap are naturally faint. As shown in Section 4.5, texture changes primarily influence prediction values. The algorithm mostly changes the area around the eyes and eyebrows to reach the reference values $\tilde{y} = 10$ and $\tilde{y} = 40$ from age 20. For the younger age, it smoothen

the skin, while for the older age, it darkens the skin and adds texture. The most apparent changes with increasing age to $\tilde{y} = 60$ and $\tilde{y} = 80$ occur around the eyes the intensity of the smile lines, and also the darkening of the skin. Moreover, we observe one of the same key features of the predictor as observed in the original ACE paper [25]: The cheek color gets redder with increasing reference value.

Diff-AE-RE in contrast produces heatmaps that are much more intuitively interpretable. We first observe that for $\tilde{y} = 10$, the regressor favors darker, rounder eyes and darker hair and skin. In addition, the neck seems to get slimmer. Noticeably, the whole image appears to be darker, which shows the problem of maintaining sparsity for this method. However, changes appear to be sparser for the latter reference values.

The transition from $\tilde{y} = 20$ to $\tilde{y} = 40$ strongly suggests the presence of a spurious feature, as the main modification is the addition of an earring, consistent with the findings in Section 4.5. Beyond this, the strongest changes appear to be in the shape of the smile and nose, along with minor changes to the lips and the width of the neck. As age progresses to $\tilde{y} = 60$, these features become even more pronounced. In addition, the jaw and neck shape gain importance, as well as the decrease in hair volume and the number of wrinkles. For $\tilde{y} = 80$, further modifications include thinning of the lips and eyebrows, complete disappearance of the second row of teeth, rounder chin, and even wider neck. The explanations provided by Diff-AE-RE reflect a combination of natural progressive aging processes and potential dataset biases.

4.7 Ablation Study

To better understand the contribution of each component of Diff-AE-RE, we conduct an ablation study. For an applicable study on AC-RE, we refer to the ablation study on ACE [25].

First, we explore the choice and distance function and its regularization constant λ_d . For this we empirically tested combinations of the ℓ_1 and ℓ_2 distance functions in the pixel and latent space, as well as a range of regularization constants $10^{-6} \leq \lambda_d \leq 10^{-2}$. We find that using no distance constraint resulted in aggressive image changes with some non-semantic changes. Applying the distance function on the pixel space results in counterfactuals with minimal changes in the image and the predicted age. Although the ℓ_2 distance limited the alterations somewhat, applying the ℓ_1 distance on the latent space produces more semantically meaningful and higher-quality counterfactuals. Regarding the regularization constant, we find that choosing $\lambda_d = 10^{-5}$ strikes a balance between generating expressive changes and preventing domination of the loss. We show examples of these effects with $\lambda_d = 10^{-5}$ in Figure 5.

Second, we evaluated the choice of the optimization algorithm. Stochastic Gradient Descent (SGD) and SGD with momentum struggled to effectively navigate the latent space, requiring impractically low learning rates. In contrast, Adam [30] efficiently optimized towards the reference value. Finally, we examine the learning rate, observing that lower rates yielded smoother and more realistic

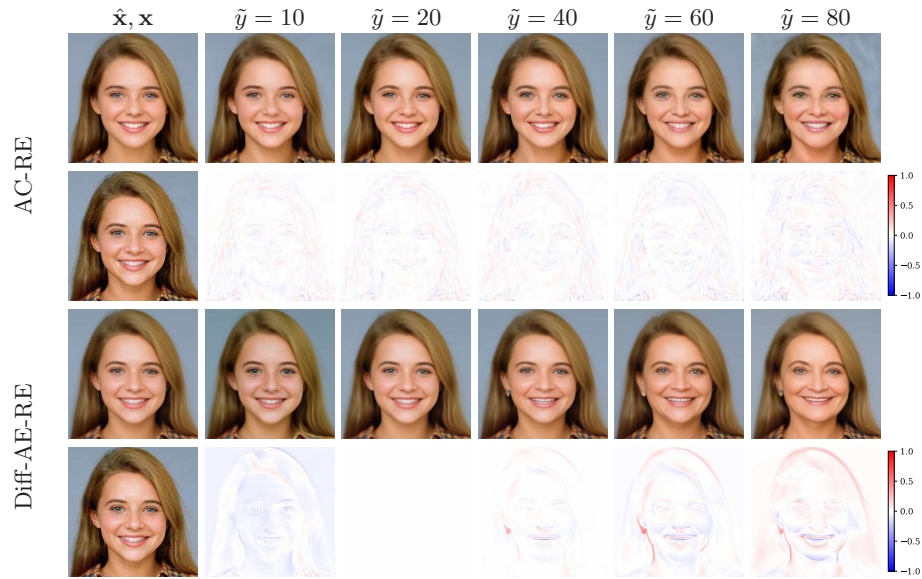


Fig. 4. Granular reference values. Counterfactual explanations generated by AC-RE and Diff-AE-RE for different reference values $\tilde{y} \in \{10, 20, 40, 60, 80\}$ for an image with an initial predicted age of 20. For each algorithm, we show the reconstructed image \hat{x} with corresponding counterfactuals input in the first row and input image x and heatmaps visualizing pixel-wise differences in the second row. AC-RE produces sparse, subtle changes. In contrast, Diff-AE-RE exhibits more intuitive but less sparse modifications for the lower age. This approach highlights key facial transformations associated with aging as well as a spurious feature

counterfactuals, while higher rates risked exiting the data manifold, leading to poor image quality. This leads us to empirically choose a learning rate of 0.002 for Adam.



Fig. 5. Effect of distance function in the latent space with $\lambda_d = 10^{-5}$ We show the input image \mathbf{x} and the generated counterfactuals with either no, ℓ_1 - and ℓ_2 -distance for the latent codes of the input \mathbf{z}_{sem} and counterfactual \mathbf{z}'_{sem} . Without a distance function, alterations are aggressive, with some non-semantic changes. While the ℓ_2 -distance somewhat limits this, ℓ_1 -distance limits changes to be semantically meaningful while increasing the quality of the explanation

5 Conclusion

In this paper, we addressed the underexplored area of counterfactual explanations for image regression tasks by proposing two novel methods utilizing diffusion-based generative models: Adversarial Counterfactual Regression Explanations (AC-RE) operating in pixel space and Diffusion Autoencoder Regression Explanations (Diff-AE-RE) operating in latent space. Our methods perform similarly to classification-based counterparts and successfully generate realistic, semantic, and smooth counterfactuals. They provide valuable insights into the decision-making process of regression models and reveal spurious correlations. We demonstrated that feature changes in regression counterfactuals are dependent on the prediction region, with larger semantic alterations required for significant value shifts. Furthermore, we observed a trade-off between sparsity and quality, with AC-RE offering greater sparsity and Diff-AE-RE providing higher quality and semantic flexibility. This research paves the way for a better understanding of image regression models. Future work can apply these techniques to state-of-the-art diffusion models [49] and examine the theoretical implications of the Diffusion Autoencoder for Diffeomorphic Counterfactuals [14].

Acknowledgments. This work was supported by **BASLEARN**—TU Berlin/BASF Joint Laboratory, co-financed by TU Berlin and BASF SE.

Disclosure of Interests. The authors have no competing interests to declare that are relevant to the content of this article.

Bibliography

- [1] Anders, C.J., Weber, L., Neumann, D., Samek, W., Müller, K.R., Lapuschkin, S.: Finding and removing Clever Hans: Using explanation methods to debug and improve deep models. *Information Fusion* **77**, 261–295 (Jan 2022). <https://doi.org/10.1016/j.inffus.2021.07.015>
- [2] Atad, M., Schinz, D., Moeller, H., Graf, R., Wiestler, B., Rueckert, D., Navab, N., Kirschke, J.S., Keicher, M.: Counterfactual Explanations for Medical Image Classification and Regression using Diffusion Autoencoder. *Machine Learning for Biomedical Imaging 2* (iMIMIC 2023 special issue), 2103–2125 (Sep 2024). <https://doi.org/10.59275/j.melba.2024-4862>
- [3] Bach, S., Binder, A., Montavon, G., Klauschen, F., Müller, K.R., Samek, W.: On pixel-wise explanations for non-linear classifier decisions by layer-wise relevance propagation. *PLoS one* **10**(7), e0130140 (2015)
- [4] Baehrens, D., Schroeter, T., Harmeling, S., Kawanabe, M., Hansen, K., Müller, K.R.: How to Explain Individual Classification Decisions. *Journal of Machine Learning Research* **11**(61), 1803–1831 (2010)
- [5] Bender, S., Anders, C.J., Chormai, P., Marxfeld, H.A., Herrmann, J., Montavon, G.: Towards Fixing Clever-Hans Predictors with Counterfactual Knowledge Distillation. In: *Proceedings of the IEEE/CVF International Conference on Computer Vision*. pp. 2607–2615 (2023)
- [6] Binder, A., Bockmayr, M., Hägele, M., Wienert, S., Heim, D., Hellweg, K., Ishii, M., Stenzinger, A., Hocke, A., Denkert, C., Müller, K.R., Klauschen, F.: Morphological and molecular breast cancer profiling through explainable machine learning. *Nature Machine Intelligence* **3**(4), 355–366 (Apr 2021). <https://doi.org/10.1038/s42256-021-00303-4>
- [7] Cao, Q., Shen, L., Xie, W., Parkhi, O.M., Zisserman, A.: VGGFace2: A Dataset for Recognising Faces across Pose and Age. In: *2018 13th IEEE International Conference on Automatic Face & Gesture Recognition (FG 2018)*. pp. 67–74. IEEE Press, Xi’an, China (May 2018). <https://doi.org/10.1109/FG.2018.00020>
- [8] Chen, K., Loy, C.C., Gong, S., Xiang, T.: Feature mining for localised crowd counting. In: *Bmvc*. vol. 1, p. 3 (2012)
- [9] Cherepkov, A., Voynov, A., Babenko, A.: Navigating the GAN Parameter Space for Semantic Image Editing. In: *2021 IEEE/CVF Conference on Computer Vision and Pattern Recognition (CVPR)*. pp. 3670–3679. IEEE, Nashville, TN, USA (Jun 2021). <https://doi.org/10.1109/CVPR46437.2021.00367>
- [10] Cohen, J.P., Brooks, R., En, S., Zucker, E., Pareek, A., Lungren, M.P., Chaudhari, A.: Gifsplanation via Latent Shift: A Simple Autoencoder Approach to Counterfactual Generation for Chest X-rays. In: *Proceedings of the Fourth Conference on Medical Imaging with Deep Learning*. pp. 74–104. PMLR (Aug 2021)

- [11] Couairon, G., Verbeek, J., Schwenk, H., Cord, M.: DiffEdit: Diffusion-based semantic image editing with mask guidance. In: The Eleventh International Conference on Learning Representations (Sep 2022)
- [12] Das, A., Rad, P.: Opportunities and Challenges in Explainable Artificial Intelligence (XAI): A Survey (Jun 2020). <https://doi.org/10.48550/arXiv.2006.11371>
- [13] Delaney, E., Pakrashi, A., Greene, D., Keane, M.T.: Counterfactual Explanations for Misclassified Images: How Human and Machine Explanations Differ (Dec 2022)
- [14] Dombrowski, A.K., Gerken, J.E., Müller, K.R., Kessel, P.: Diffeomorphic Counterfactuals With Generative Models. *IEEE Transactions on Pattern Analysis and Machine Intelligence* **46**(5), 3257–3274 (May 2024). <https://doi.org/10.1109/TPAMI.2023.3339980>
- [15] Image Editor | getimg.ai
- [16] Guidotti, R.: Counterfactual explanations and how to find them: Literature review and benchmarking. *Data Mining and Knowledge Discovery* **38**(5), 2770–2824 (Apr 2022). <https://doi.org/10.1007/s10618-022-00831-6>
- [17] Hesse, L.S., Dinsdale, N.K., Namburete, A.I.: Prototype Learning for Explainable Brain Age Prediction. In: 2024 IEEE/CVF Winter Conference on Applications of Computer Vision (WACV). pp. 7888–7898. IEEE, Waikoloa, HI, USA (Jan 2024). <https://doi.org/10.1109/WACV57701.2024.00772>
- [18] Heusel, M., Ramsauer, H., Unterthiner, T., Nessler, B., Hochreiter, S.: GANs Trained by a Two Time-Scale Update Rule Converge to a Local Nash Equilibrium. In: *Advances in Neural Information Processing Systems*. vol. 30. Curran Associates, Inc. (2017)
- [19] Ho, J., Jain, A., Abbeel, P.: Denoising diffusion probabilistic models. In: *Proceedings of the 34th International Conference on Neural Information Processing Systems*. pp. 6840–6851. NIPS '20, Curran Associates Inc., Red Hook, NY, USA (Dec 2020)
- [20] Huang, G., Liu, Z., Van Der Maaten, L., Weinberger, K.Q.: Densely Connected Convolutional Networks. In: 2017 IEEE Conference on Computer Vision and Pattern Recognition (CVPR). pp. 2261–2269. IEEE, Honolulu, HI (Jul 2017). <https://doi.org/10.1109/CVPR.2017.243>
- [21] Huberman-Spiegelglas, I., Kulikov, V., Michaeli, T.: An Edit Friendly DDPM Noise Space: Inversion and Manipulations (Apr 2024)
- [22] Hvilshøj, F., Iosifidis, A., Assent, I.: On Quantitative Evaluations of Counterfactuals (Oct 2021)
- [23] Jacob, P., Zablocki, É., Ben-Younes, H., Chen, M., Pérez, P., Cord, M.: STEEX: Steering Counterfactual Explanations with Semantics (Jul 2022)
- [24] Jeanneret, G., Simon, L., Jurie, F.: Diffusion Models for Counterfactual Explanations (Mar 2022). <https://doi.org/10.48550/arXiv.2203.15636>
- [25] Jeanneret, G., Simon, L., Jurie, F.: Adversarial Counterfactual Visual Explanations. In: 2023 IEEE/CVF Conference on Computer Vision and Pattern Recognition (CVPR). pp. 16425–16435. IEEE, Vancouver, BC, Canada (Jun 2023). <https://doi.org/10.1109/CVPR52729.2023.01576>

- [26] Jeanneret, G., Simon, L., Jurie, F.: Text-to-Image Models for Counterfactual Explanations: A Black-Box Approach (Nov 2023)
- [27] Karras, T., Aila, T., Laine, S., Lehtinen, J.: Progressive Growing of GANs for Improved Quality, Stability, and Variation (Feb 2018). <https://doi.org/10.48550/arXiv.1710.10196>
- [28] Karras, T., Laine, S., Aila, T.: A style-based generator architecture for generative adversarial networks. In: Proceedings of the IEEE/CVF Conference on Computer Vision and Pattern Recognition (CVPR) (Jun 2019)
- [29] Khan, T., Ahmad, K., Khan, J., Khan, I., Ahmad, N.: An Explainable Regression Framework for Predicting Remaining Useful Life of Machines (Apr 2022)
- [30] Kingma, D.P., Ba, J.: Adam: A Method for Stochastic Optimization (Jan 2017). <https://doi.org/10.48550/arXiv.1412.6980>
- [31] Kingma, D.P., Welling, M.: Auto-Encoding Variational Bayes (Dec 2022). <https://doi.org/10.48550/arXiv.1312.6114>
- [32] Klauschen, F., Dippel, J., Keyl, P., Jurmeister, P., Bockmayr, M., Mock, A., Buchstab, O., Alber, M., Ruff, L., Montavon, G., Müller, K.R.: Toward Explainable Artificial Intelligence for Precision Pathology. *Annual Review of Pathology: Mechanisms of Disease* **19**(1), 541–570 (Jan 2024). <https://doi.org/10.1146/annurev-pathmechdis-051222-113147>
- [33] Kwon, M., Jeong, J., Uh, Y.: Diffusion Models already have a Semantic Latent Space (Mar 2023)
- [34] Lapuschkin, S., Binder, A., Müller, K.R., Samek, W.: Understanding and Comparing Deep Neural Networks for Age and Gender Classification. In: Proceedings of the IEEE International Conference on Computer Vision Workshops. pp. 1629–1638 (2017)
- [35] Lapuschkin, S., Wäldchen, S., Binder, A., Montavon, G., Samek, W., Müller, K.R.: Unmasking Clever Hans predictors and assessing what machines really learn. *Nature Communications* **10**(1), 1096 (Mar 2019). <https://doi.org/10.1038/s41467-019-08987-4>
- [36] Letzgus, S., Müller, K.R.: An explainable AI framework for robust and transparent data-driven wind turbine power curve models. *Energy and AI* **15**, 100328 (Jan 2024). <https://doi.org/10.1016/j.egyai.2023.100328>
- [37] Letzgus, S., Müller, K.R., Montavon, G.: XpertAI: Uncovering model strategies for sub-manifolds (Mar 2024). <https://doi.org/10.48550/arXiv.2403.07486>
- [38] Letzgus, S., Wagner, P., Lederer, J., Samek, W., Müller, K.R., Montavon, G.: Toward Explainable AI for Regression Models. *IEEE Signal Processing Magazine* **39**(4), 40–58 (Jul 2022). <https://doi.org/10.1109/MSP.2022.3153277>
- [39] Lin, Y., Shen, J., Wang, Y., Pantic, M.: FP-age: Leveraging face parsing attention for facial age estimation in the wild. *arXiv* (2021)
- [40] Ling, H., Kreis, K., Li, D., Kim, S.W., Torralba, A., Fidler, S.: EditGAN: High-Precision Semantic Image Editing (Nov 2021). <https://doi.org/10.48550/arXiv.2111.03186>

- [41] Lugmayr, A., Danelljan, M., Romero, A., Yu, F., Timofte, R., Van Gool, L.: RePaint: Inpainting using Denoising Diffusion Probabilistic Models. In: 2022 IEEE/CVF Conference on Computer Vision and Pattern Recognition (CVPR). pp. 11451–11461. IEEE, New Orleans, LA, USA (Jun 2022). <https://doi.org/10.1109/CVPR52688.2022.01117>
- [42] Lundberg, S.M., Lee, S.I.: A Unified Approach to Interpreting Model Predictions. In: Advances in Neural Information Processing Systems. vol. 30. Curran Associates, Inc. (2017)
- [43] Madry, A., Makelov, A., Schmidt, L., Tsipras, D., Vladu, A.: Towards Deep Learning Models Resistant to Adversarial Attacks (Sep 2019). <https://doi.org/10.48550/arXiv.1706.06083>
- [44] Molnar, C.: Interpretable Machine Learning. A Guide for Making Black Box Models Explainable. Leanpub, 2 edn. (2022)
- [45] Preechakul, K., Chatthee, N., Wizadwongsa, S., Suwajanakorn, S.: Diffusion Autoencoders: Toward a Meaningful and Decodable Representation. In: 2022 IEEE/CVF Conference on Computer Vision and Pattern Recognition (CVPR). pp. 10609–10619. IEEE, New Orleans, LA, USA (Jun 2022). <https://doi.org/10.1109/CVPR52688.2022.01036>
- [46] Raman, C., Nonnemaker, A., Villegas-Morcillo, A., Hung, H., Loog, M.: Why Did This Model Forecast This Future? Information-Theoretic Saliency for Counterfactual Explanations of Probabilistic Regression Models. Advances in Neural Information Processing Systems **36**, 33222–33240 (Dec 2023)
- [47] Ribeiro, M.T., Singh, S., Guestrin, C.: "Why Should I Trust You?": Explaining the Predictions of Any Classifier. In: Proceedings of the 22nd ACM SIGKDD International Conference on Knowledge Discovery and Data Mining. pp. 1135–1144. KDD '16, Association for Computing Machinery, New York, NY, USA (Aug 2016). <https://doi.org/10.1145/2939672.2939778>
- [48] Rodríguez, P., Caccia, M., Lacoste, A., Zamparo, L., Laradji, I., Charlin, L., Vazquez, D.: Beyond Trivial Counterfactual Explanations With Diverse Valuable Explanations. In: Proceedings of the IEEE/CVF International Conference on Computer Vision. pp. 1056–1065 (2021)
- [49] Rombach, R., Blattmann, A., Lorenz, D., Esser, P., Ommer, B.: High-Resolution Image Synthesis with Latent Diffusion Models (Apr 2022). <https://doi.org/10.48550/arXiv.2112.10752>
- [50] Rothe, R., Timofte, R., Gool, L.V.: DEX: Deep EXpectation of Apparent Age from a Single Image. In: 2015 IEEE International Conference on Computer Vision Workshop (ICCVW). pp. 252–257. IEEE, Santiago, Chile (Dec 2015). <https://doi.org/10.1109/ICCVW.2015.41>
- [51] Samek, W., Montavon, G., Lapuschkin, S., Anders, C.J., Müller, K.R.: Explaining Deep Neural Networks and Beyond: A Review of Methods and Applications. Proceedings of the IEEE **109**(3), 247–278 (Mar 2021). <https://doi.org/10.1109/JPROC.2021.3060483>
- [52] Samek, W., Müller, K.R.: Towards Explainable Artificial Intelligence. In: Samek, W., Montavon, G., Vedaldi, A., Hansen, L.K., Müller, K.R. (eds.) Explainable AI: Interpreting, Explaining and Visualizing Deep

- Learning, pp. 5–22. Springer International Publishing, Cham (2019). https://doi.org/10.1007/978-3-030-28954-6_1
- [53] Singla, S., Eslami, M., Pollack, B., Wallace, S., Batmanghelich, K.: Explaining the black-box smoothly—A counterfactual approach. *Medical Image Analysis* **84**, 102721 (Feb 2023). <https://doi.org/10.1016/j.media.2022.102721>
- [54] Song, J., Meng, C., Ermon, S.: Denoising Diffusion Implicit Models. In: *International Conference on Learning Representations* (Oct 2020)
- [55] Spooner, T., Dervovic, D., Long, J., Shepard, J., Chen, J., Magazzeni, D.: Counterfactual Explanations for Arbitrary Regression Models. *ArXiv* (Jun 2021)
- [56] Sundararajan, M., Taly, A., Yan, Q.: Axiomatic Attribution for Deep Networks. In: *Proceedings of the 34th International Conference on Machine Learning*. pp. 3319–3328. PMLR (Jul 2017)
- [57] Szegedy, C., Zaremba, W., Sutskever, I., Bruna, J., Erhan, D., Goodfellow, I., Fergus, R.: Intriguing properties of neural networks (Feb 2014). <https://doi.org/10.48550/arXiv.1312.6199>
- [58] Van Der Velden, B.H.M., Janse, M.H.A., Ragusi, M.A.A., Loo, C.E., Gilhuijs, K.G.A.: Volumetric breast density estimation on MRI using explainable deep learning regression. *Scientific Reports* **10**(1), 18095 (Oct 2020). <https://doi.org/10.1038/s41598-020-75167-6>
- [59] Verma, S., Dickerson, J., Hines, K.: Counterfactual Explanations for Machine Learning: A Review. *NeurIPS 2020 Workshop: ML Retrospectives, Surveys & Meta-Analyses (ML-RSA)* (2020)
- [60] Wachter, S., Mittelstadt, B., Russell, C.: Counterfactual Explanations Without Opening the Black Box: Automated Decisions and the GDPR (Oct 2017). <https://doi.org/10.2139/ssrn.3063289>
- [61] Zeiler, M.D., Fergus, R.: Visualizing and Understanding Convolutional Networks. In: Fleet, D., Pajdla, T., Schiele, B., Tuytelaars, T. (eds.) *Computer Vision – ECCV 2014*. pp. 818–833. Springer International Publishing, Cham (2014). https://doi.org/10.1007/978-3-319-10590-1_53
- [62] Zhou, B., Khosla, A., Lapedriza, A., Oliva, A., Torralba, A.: Learning Deep Features for Discriminative Localization. In: *Proceedings of the IEEE Conference on Computer Vision and Pattern Recognition*. pp. 2921–2929 (2016)